

RESEARCH ARTICLE

Robust Lyapunov-based motion control of a redundant upper limb cable-driven rehabilitation robot

Niloufar Sadat Seyfi and Ali Keymasi Khalaji* 

Department of Mechanical Engineering, Faculty of Engineering, Kharazmi University, Tehran, 15719-14911, Iran

*Corresponding author. E-mail: keymasi@khu.ac.ir

Received: 15 August 2021; **Revised:** 9 January 2022; **Accepted:** 6 February 2022; **First published online:** 14 March 2022

Keywords: cable-driven rehabilitation robot, Lyapunov-based control, robustness, positive cable forces, joint limit avoidance, computed-torque-like control with independent-joint compensation

Abstract

This research presents an upper limb cable-driven rehabilitating robot with one degree of redundancy to improve the movements of the injured. A spatial trajectory is planned through the joint limit avoidance approach to apply the limits of the joint angles, which is a new method for trajectory planning of joints with an allowed definite interval. Firstly, a Lyapunov-based control is applied to the robot with taking uncertainty and disturbances into consideration. To derive the best responses of the system with considering uncertainty and disturbances, a novel robust tracking controller, namely a computed-torque-like with independent-joint compensation, is introduced. The mentioned new robust controller has not been applied to any cable robot which is the novelty of this paper to derive a superior output and the robustness of the given approach. Stability analysis of both controllers is demonstrated and the outputs of the controllers are compared for an exact three-dimensional motion planning and desirable cable forces. Eventually, the proposed novel controller revealed a better function in the presence of uncertainties and disturbances with about 28.21% improvement in tracking errors and 69.22% improvement in the required cable forces as control inputs, which is a considerable figure.

1. Introduction

Conventional treatments in rehabilitation depend on the existence of the number of therapists to help the patients, which consume time and energy and do not sound economical [1]. Robotic rehabilitation systems bring a wide range of merits and can improve accuracy and efficiency, as well as make the system controllable and reduce the necessity of the assistance of physiotherapists [1]. In the last decades, the majority of rehabilitation exoskeletons were made of rigid links, which have a high weight and inflexibility [2]. MIT-MANUS is one of the first rehabilitation robots, which was first time launched by MIT University, and consists of a five-link robot with two degrees of freedom (DOFs) in the plane [2]. MIME at Stanford University has six DOFs and is able to lead the injured arm to pursue the predefined trajectory [2]. The CADEN-7, an upper limb rehabilitation system, can produce motion with seven DOFs in the shoulder, elbow, and wrist [2]. The REPERT, an arm motion-aided training system by Arizona State University, consumes pneumatic artificial muscles to guide a five-DOF motion of the arm [2]. Since rehabilitation systems have some demerits, such as smaller workspace, inflexibility, higher expenses of construction, and higher inertia [1], many essays in cable-driven upper limb robots have been undertaken [3–5]. A three-DOF exoskeleton cable-driven rehabilitation robot (CDRR) has been made to boost the arm movement of the patients [6]. Zannotto et al. [7] studied Sophia-3, an end-effector-based cable-actuated rehabilitation system to help motions in the plane. Besides, a lightweight wire-driven rehabilitation system has been studied to help the movements of shoulder and elbow joints [8]. A CDRR was made of a frame, cables, and an end-effector in which cables were driven through motors [9]. A planar 4-CDRR was also made in 2014 [9].

The control method is one of the most vital subjects that impact the function of the robots and the accuracy of the trajectory tracking with the least error. Some of them with various controllers are presented below.

An adaptive admittance control was studied on a manipulator with task space constraints to prepare compliance with external forces [10]. Mao and Agrawal [11] designed a force control of a cable-driven upper limb rehabilitating system. Similarly, in 2011, impedance control was applied to a rehabilitation system through a Lyapunov approach [12]. In a different work, taking advantage of an admittance control for a guide control was confirmed to be capable to move the human upper limb through virtual guidelines in a rehabilitation system [13]. Furthermore, a novel method was designed for upper limb exoskeleton robot through Muscle Circumference Sensor with the force sensors to estimate the human interactive force through an adaptive impedance controller [14]. A new torque-field controller was applied to a cable-driven wrist rehabilitation system to provide motion training [15]. In another research, an admittance control was used for an upper limb cable-driven rehabilitating system with three DOFs in three-dimensional (3D) motion to track the desirable trajectory without any reference trajectory [16]. A neurological rehabilitation device was presented to provide patients to perform different motions using an impedance-based control [17]. As can be seen, force, impedance, and admittance controllers are widely consumed in different CDRRs, and a minority of researchers have worked on robust motion controls with considering uncertainty and disturbance. Some of the papers have studied motion controls in cable rehabilitation systems but have not worked on the robustness of the system with considering uncertainty and disturbance, which are mentioned below.

In ref. [18], motion and force controls are studied in a seven-DOF cable-driven rehabilitation training robot, and both active and passive rehabilitation training modes are suggested for enhancement of the movements of the patients. Xiong and Diao [19] worked on motion control for the safety of a cable-driven parallel manipulator in rehabilitation devices with large deformation cables and position-controlling actuators. Consequently, ref. [2] proposed the tracking control of a four-DOF cable-driven upper limb robot to move the whole upper limb along desired trajectories. Moreover, inverse dynamics modeling was designed for a new rehabilitating system with a parallel joint for tracking the reference trajectory [20]. In 2020, a new four-DOF robotic cable-driven upper limb robot with pneumatic artificial muscle actuators was studied and motion control was applied for the trajectory control [21]. Also, ref. [22] suggested a hybrid active force and position controller of an upper limb cable-driven rehabilitating system with human movement intention detection, which has been considered as the desired position and velocity.

To prove the effectiveness of applying a robust controller in a similar system, a polynomial-based robust adaptive impedance control method for electrically driven robots is introduced in ref. [23]. Polynomials of degree N as an approximator for uncertainties, unmodeled dynamics, and external disturbances indicated superior performance in position control due to the robustness of the given control algorithm. Since a robust controller such as an optimal robust voltage control presented in ref. [24] showed its efficiency in tracking errors for electrically driven robot manipulators in the presence of uncertainty, this paper introduces a novel robust motion control, namely computed-torque-like control with independent-joint compensation while taking uncertainty and disturbance into consideration, which is the novelty of this paper to reveal the robustness of the given approach.

One of the concerns of this paper is to improve the lower limb movements by a rehabilitation system on spatial trajectories, in which the path is planned through a new method, called joint limit avoidance (JLA). Furthermore, since few numbers of papers have worked on robust motion control of cable rehabilitation systems in a 3D path planning in front of uncertainties and disturbances, the main goal of this research is the presentation of this new robust controller.

The kinematic formulation of cables has been exploited in Section 2. The dynamic formulation has been derived through the Lagrangian method in Section 3. The unilateral cable force, which is one of the challenging parts of cable robots, is obtained in Section 4. Section 5 is allocated to a new path planning approach to keep the joints in their allowed interval. In Section 6, a Lyapunov-based control

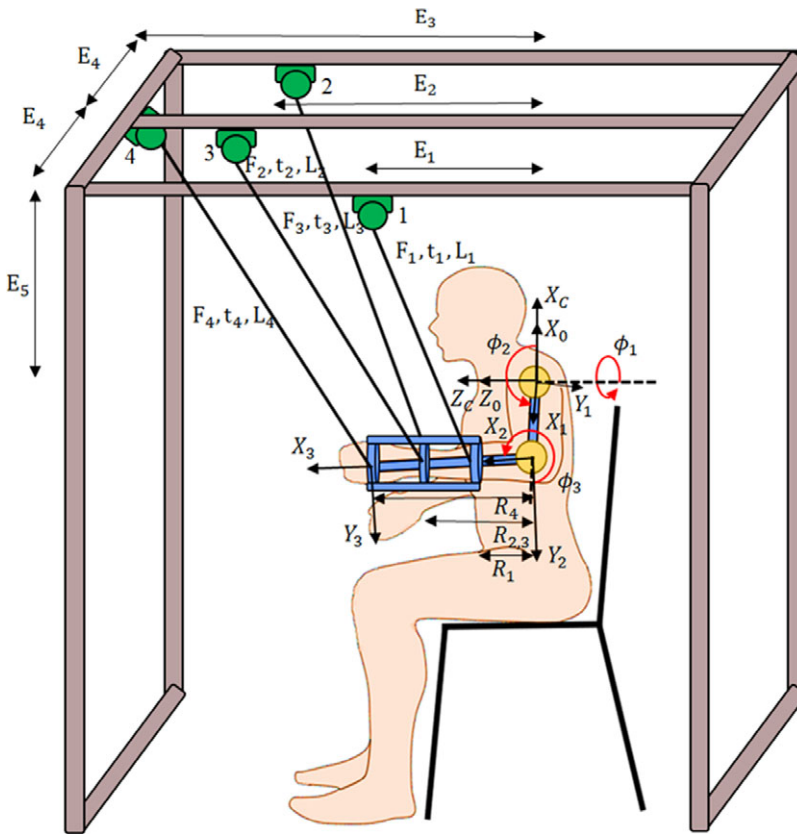


Figure 1. The proposed upper limb cable-driven rehabilitation robot scheme.

and a computed-torque-like control with an independent-joint compensator are designed and compared with considering uncertainties and disturbances. At last, the conclusion has been written in Section 9.

2. Kinematic formulation of the upper limb CDRR

In this upper limb cable-driven rehabilitation system, {0} and {1} are local coordinate systems on the shoulder joint and {2} on the elbow, and {3} is located on the mass center of the palm, as can be seen in Fig. 1. These formulations, L_i are indicators of cable lengths and t_i are related to unit vectors. Besides, E_i show motors' positions connected to the reference frame {C} and R_i is the vector that indicates the distance from the points of cable connection to the joints. Jacobian matrix J_c connects joint velocity to the \dot{L} cable velocity. m_a introduces arm mass; m_f and m_h are also forearm and hand masses, respectively. Robot parameters are written in Table I.

Cable length, L_i , can be calculated geometrically as

$$E_i - R_i = L_i t_i \quad . \quad i = 1 \rightarrow 5 \tag{1}$$

where t_i represents unit vectors of the cables. Derivation of Eq. (1) to time results in

$$\frac{\partial L_i}{\partial t} t_i = \frac{\partial E_i}{\partial t} - \frac{\partial R_i}{\partial \phi} \frac{\partial \phi}{\partial t} \tag{2}$$

Table I. Figures for the upper limb cable-driven rehabilitating system and human upper limb.

Parameter	Value	Unit	Parameter	Value	Unit
E_1	0.6	m	R_1	0.1	m
E_2	0.9	m	R_2	0.2	m
E_3	1.4	m	R_3	0.2	m
E_4	0.5	m	R_4	0.38	m
E_5	1	m	m_a	3.25	kg
l_a	0.323	m	m_f	1.87	kg
l_f	0.29	m	m_h	0.65	kg
l_h	0.2	m			

where E_i is the constant and thus $\frac{\partial E_i}{\partial \phi} = 0$. Multiplying Eq. (2) in t_i^T yields

$$\dot{L}_i t_i^T = -t_i^T \frac{\partial R_i}{\partial \phi} \dot{\phi} \tag{3}$$

where $\frac{\partial R_i}{\partial \phi}$ defines a Jacobian matrix of the cables J_c , therefore

$$\dot{L}_i = -t_i^T J_c \dot{\phi} \tag{4}$$

where $\dot{\phi} = [\dot{\phi}_1 \ \dot{\phi}_2 \ \dot{\phi}_3]^T$ shows joint velocities, $\phi = [\phi_1 \ \phi_2 \ \phi_3]^T$ introduces generalized coordinates, and F_i are cable forces. ϕ_1 represents abduction/adduction of the shoulder joint in the frontal plane, while ϕ_2 and ϕ_3 are flexion/extension of the shoulder and elbow joints, respectively, in the sagittal plane. The proposed upper limb rehabilitation system is depicted in Fig. 1.

The mentioned CDRR has three DOFs. It works through five cables run by five motors attached to the system frame, and cables have been connected to the orthosis with cuffs.

3. Dynamic equations

The system has three DOFs with flexion/extension of shoulder and elbow joints in the sagittal plane and abduction/adduction of the shoulder joint in the frontal plane, while the wrist is considered to be constant. The dynamic formulation of the system is obtained through the Lagrange formulation. The general dynamic formulation is written as

$$M(\phi)\ddot{\phi} + B(\phi, \dot{\phi})\dot{\phi} + G(\phi) = T \tag{5}$$

where $M(\phi)$ represents the positive-definite mass matrix, and $B(\phi, \dot{\phi})$ illustrates centrifugal and Coriolis forces vector. $G(\phi)$ entails gravitational forces, while T in Eq. (6) is an indicator of the system joint torques.

$$T = J_c^T (F + \Omega) \tag{6}$$

where Ω indicates system external disturbances and cable forces are considered as $F = [F_1 \ F_2 \ F_3 \ F_4 \ F_5]^T$. J_c shows the Jacobian matrix, which maps cable tensions to the joint torques. Thus,

$$M(\phi)\ddot{\phi} + B(\phi, \dot{\phi})\dot{\phi} + G(\phi) = J_c^T (F + \Omega) \tag{7}$$

where

$$J_{ci} = \begin{bmatrix} \frac{\partial R_{ix}}{\partial \phi_1} & \frac{\partial R_{ix}}{\partial \phi_2} & \frac{\partial R_{ix}}{\partial \phi_3} \\ \frac{\partial R_{iy}}{\partial \phi_1} & \frac{\partial R_{iy}}{\partial \phi_2} & \frac{\partial R_{iy}}{\partial \phi_3} \\ \frac{\partial R_{iz}}{\partial \phi_1} & \frac{\partial R_{iz}}{\partial \phi_2} & \frac{\partial R_{iz}}{\partial \phi_3} \end{bmatrix}, i = 1 \rightarrow 5 \tag{8}$$

And the vector J_c^T is defined as

$$J_c^T = [J_{c1}^T t_1 J_{c2}^T t_2 J_{c3}^T t_3 J_{c4}^T t_4 J_{c5}^T t_5] \tag{9}$$

4. Unilateral cable tension

Since only positive forces are feasible for controlling the cable systems, one of the tough issues in cable systems is applying unilateral cable tension. This challenge can be resolved through the null space of a Jacobian matrix in a redundant cable robot. A redundant cable robot is a system in which at least one cable is more than the DOF. Control input vector can be defined as ref. [25]

$$F = F_p + F_h \tag{10}$$

where F_p is the particular solution and can be derived from the dynamic Eq. (7) as

$$F_p = (J_c^T)^\# \{M(\phi)\ddot{\phi} + B(\phi, \dot{\phi})\dot{\phi} + G(\phi)\} \tag{11}$$

J_c^T is a nonquadratic matrix; as a result, the pseudo-inverse of J_c^T is chosen as

$$(J_c^T)^\# = J_c(J_c^T J_c)^{-1} \tag{12}$$

If J_c^T is a full-rank matrix, Eq. (7) would have a large number of solutions. F_h in Eq. (10) is an indicator of the homogenous solution which is calculated as

$$F_h = \xi_{JT} \lambda \tag{13}$$

where ξ_{JT} introduces the null space of J_c^T , which is an $(v \times q)$ matrix. Also, v is the number of inputs. $q = v - p$ defines the degree of redundancy, p indicates the DOF, and λ shows a random $(q \times 1)$ vector. The positive condition of control inputs is ensured when λ is placed in a possible region (P_r). Wherever the whole null-space arrays get a similar sign, λ arrays would be placed in the mentioned possible region. Eventually, $F \geq 0$ is obtained:

$$F = F_p + \xi_{JT} \lambda \geq 0 \tag{14}$$

In this upper limb cable-driven rehabilitating system, one redundant cable yields a λ and four linear inequalities in Eq. (15).

$$\begin{bmatrix} F_{p1} \\ F_{p2} \\ F_{p3} \\ F_{p4} \end{bmatrix} + \begin{bmatrix} \xi_{11} \\ \xi_{21} \\ \xi_{31} \\ \xi_{41} \end{bmatrix} \lambda \geq 0 \tag{15}$$

By transformation of inequalities to equalities in six pairs of linear equations and finding intersections in every pair of equations, possible region (P_r) and a suitable λ for a positive cable force can be found. The resulted area, between solution points, is the possible area where if the resulting points satisfy all the remained equations, the appropriate λ is calculated, which can result in positive cable tensions in Eq. (14).

Table II. Allowed movement interval of hand joints.

Joint angles	Movement interval of each joint
ϕ_1	$(-40, 100)^\circ$
ϕ_2	$(0, 200)^\circ$
ϕ_3	$(210, 360)^\circ$

5. Joint limit avoidance

To control the systems which have a definite interval for the joints to move, the desired trajectories are planned through a new approach, the JLA. The upper and lower bounds of the human upper limb are written in Table II.

Generally, robots require higher joint velocities nearby a singular area, and providing these high joint rates is not possible for the motors.

Redundant manipulators can take advantage of the extra DOFs to keep their joints in the allowed intervals and away from singular areas of the end-effector, namely the main task. For redundancy resolution, a cost function is considered, which is based on minimization [25].

$$N = (J_E \dot{\phi} - \dot{X}_d)^T L_E (J_E \dot{\phi} - \dot{X}_d) + (J_A \dot{\phi} - \dot{v}_d)^T L_A (J_A \dot{\phi} - \dot{v}_d) + \dot{\phi}^T L_S \dot{\phi} \tag{16}$$

The mentioned cost function, X , represents the end-effector position vector and \dot{X} illustrates its velocity. \dot{v} is an indicator of the additional tasks. Mainly, the reference path of the end-effector (X_d) is representative of the main task, and desirable velocities of main and additional tasks are \dot{X}_d and \dot{v}_d , respectively. Moreover, \dot{X} is derived using the forward kinematic equations as

$$\dot{X} = J_E \dot{\phi} \tag{17}$$

J_E represents the end-effector Jacobian; besides

$$\dot{v} = J_A \dot{\phi} \tag{18}$$

Due to the existence of limits on hand joints, the additional task has been defined as the joint position vector.

$$v = \phi \tag{19}$$

The Jacobian matrix J_A for the additional task is shown as:

$$J_A = \frac{\partial v}{\partial \phi} = \begin{bmatrix} 1 & 0 & 0 \\ 0 & \ddots & 0 \\ 0 & 0 & 1 \end{bmatrix} \tag{20}$$

Near the joint intervals the JLA becomes active, and joint rates get zero. Afterward, joints' velocities move to the center of their allowed interval. Thus, the desired joints' rates \dot{v}_d vanish, as soon as the JLA works.

$$\dot{v}_d = 0 \tag{21}$$

Then, $\dot{\phi}$ is defined to decline the errors and the additional task rates. In the cost function in Eq. (16), the first term decreases the velocity errors of the main task, while the second term declines the additional task respectively. The third term decreases high joint rates and results in singularity avoidance. Besides, L_E , L_A , and L_S in Eq. (16) introduce diagonal positive-definite weight matrices, which represent the velocity of the end-effector, the velocity of the additional task, and singularity avoidance, respectively.

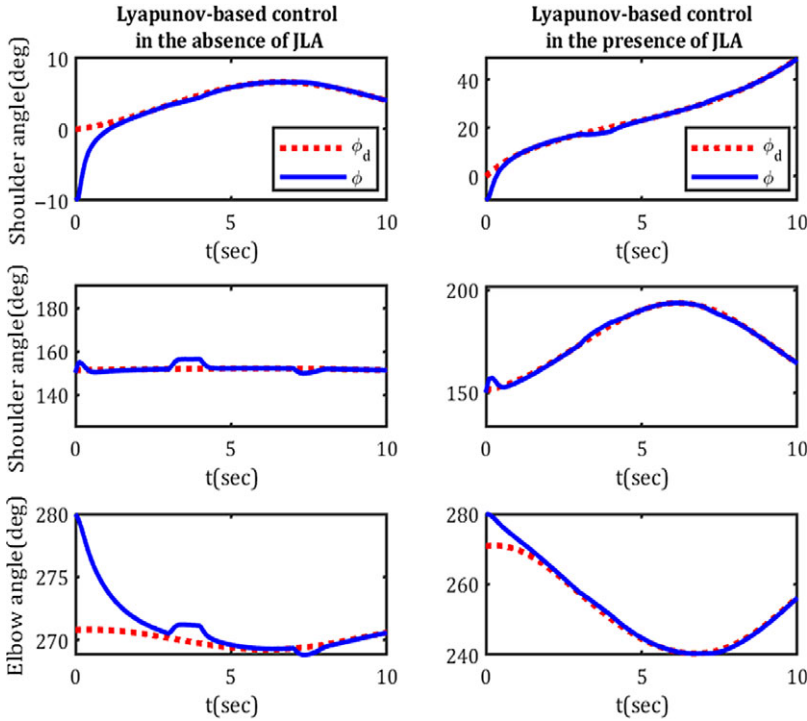


Figure 2. Path planning of hand joints in the absence and the presence of the JLA approach.

The JLA approach is activated and inactivated using the weight matrix, L_A . A desirable joint path is derived by the definition of the weight matrix L_A as a continuous function presented below

$$L_A = \begin{cases} b_0 & \phi_i < \phi_{i \min} \\ \frac{b_0}{2} \left\{ 1 + \cos \left(\pi \left(\frac{\phi_i - \phi_{i \min}}{\rho_i} \right) \right) \right\} & \phi_{i \min} \leq \phi_i \leq \phi_{i \min} + \rho_i \\ 0 & \phi + \rho_i < \phi_i < \phi_{i \max} - \rho_i \\ \frac{b_0}{2} \left\{ 1 + \cos \left(\pi \left(\frac{\phi_{i \max} - \phi_i}{\rho_i} \right) \right) \right\} & \phi_{i \max} - \rho_i \leq \phi_i \leq \phi_{i \max} \\ b_0 & \phi_i > \phi_{i \max} \end{cases} \quad (22)$$

where b_0 shows a constant coefficient. Clearly, L_A vanishes in the center of the bounds. At the moment the joint angle is placed in ρ_i , the weight matrix L_A rises from the center of the interval to the maximum value at the bounds. Joint rates would be derived through minimization of the cost function as

$$\frac{\partial N}{\partial \dot{\phi}^T} = 2 (J_E^T L_E J_E + J_A^T L_A J_A + L_S) \dot{\phi} + 2 (J_E^T L_E \dot{X}_d + J_A^T L_A \dot{v}_d) = 0 \quad (23)$$

Thus,

$$\dot{\phi} = (J_E^T L_E J_E + J_A^T L_A J_A + L_S)^{-1} (J_E^T L_E \dot{X}_d + J_A^T L_A \dot{v}_d) \quad (24)$$

Equation (24) is exploited in the recursive form as

$$\phi_d = \phi_{d-1} + (J_E^T L_E J_E + J_A^T L_A J_A + L_S)^{-1} (J_E^T L_E (X - X_1)) \quad (25)$$

X illustrates the end-effector’s position in a previous moment.

Path planning of a Lyapunov-based control is revealed in Fig. 2 to highlight the differences of joint angles in the presence and absence of the JLA approach.

Gain differential and proportional matrices are $K_D = \text{diag}\{90, 90, 90\}$ and $K_P = \text{diag}\{90, 90, 90\}$, and initial condition is defined as $\phi_0 = [-10 \ 150 \ 280]^T$, which are all the same in both conditions.

Taking advantage of the JLA method leads to the movements of the joints in their allowed upper and lower bounds and prevents their deviation.

6. Motion control schemes

In this upper limb cable-driven rehabilitating system, a Lyapunov-based controller and a novel robust motion controller, called computed-torque-like control with independent-joint compensation, are presented. A motion control utilizes actuator torques to follow the desired trajectory and minimization of the end-effector errors.

6.1. Lyapunov-based control

This Lyapunov-based control is a tracking control, which is predicted to have superior and robust performance concerning the other tracking controllers. The dynamic equation is written in Eq. (26) ref. [26].

$$T = M(\phi)\ddot{\phi} + B(\phi, \dot{\phi})\dot{\phi} + G(\phi) \tag{26}$$

The control input is defined as ref. [26]

$$T = M(\phi)\ddot{\phi}_s + B(\phi, \dot{\phi})\dot{\phi}_s + G(\phi) - K_D\dot{e} - K_Pe \tag{27}$$

where e is

$$e = \phi - \phi_d \tag{28}$$

Where $\dot{\phi}_s$ in Eq. (27) is presented as

$$\dot{\phi}_s = \dot{\phi}_d - \varepsilon e, \varepsilon > 0 \tag{29}$$

where ε is a positive constant. By taking the time derivative of Eq. (29) and replacing $\dot{\phi}_s$ and $\ddot{\phi}_s$ in Eq. (27), T is calculated

$$T = M(\phi)\ddot{\phi}_d - \varepsilon M(\phi)\dot{e} + B(\phi, \dot{\phi})\dot{\phi}_d - \varepsilon B(\phi, \dot{\phi})e + G(\phi) - K_D\dot{e} - K_Pe \tag{30}$$

By replacing the control input Eq. (27) in the dynamic equation Eq. (26), the plant or system dynamic model is

$$\ddot{\phi} = M(\phi)^{-T} (T - B(\phi, \dot{\phi})\dot{\phi} - G(\phi)) \tag{31}$$

Also, after replacing the control input in Eq. (26) the given equation is exploited

$$M(\phi)\ddot{e} + \varepsilon M(\phi)\dot{e} + B(\phi, \dot{\phi})\dot{e} + \varepsilon B(\phi, \dot{\phi})e + G(\phi) + K_D\dot{e} + K_Pe = 0 \tag{32}$$

Now \ddot{e} can be derived as

$$\ddot{e} = -\varepsilon\dot{e} - M(\phi)^{-1} (B(\phi, \dot{\phi})\dot{e} - \varepsilon B(\phi, \dot{\phi})e - G(\phi) - K_D\dot{e} - K_Pe) \tag{33}$$

The Lyapunov function is considered as

$$H = \frac{1}{2} \begin{bmatrix} e^T & \dot{e}^T \end{bmatrix} \begin{bmatrix} \varepsilon K_D + K_P + \varepsilon^2 M(\phi) & \varepsilon M(\phi) \\ \varepsilon M(\phi) & M(\phi) \end{bmatrix} \begin{bmatrix} e \\ \dot{e} \end{bmatrix} = \frac{1}{2} D^T W D \tag{34}$$

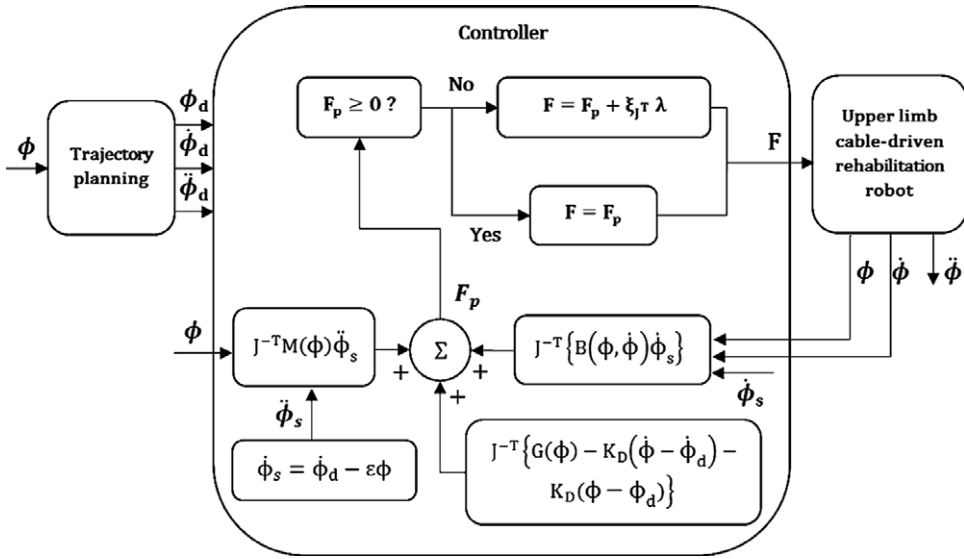


Figure 3. The diagram of the Lyapunov-based control for the upper limb cable rehabilitating robot.

which $D = [e^T \quad \dot{e}^T]^T$, and W is a positive-definite matrix. Using some properties such as $[e \quad \dot{e}^T]^T = [\dot{e}^T \quad e]^T$, $MM^{-1} = I$ and $O^T (\dot{M} - 2B) O = 0$, where O is an arbitrary vector, \dot{H} can be obtained as

$$\begin{aligned} \dot{H} = & \varepsilon K_D \dot{e}^T e + K_p \dot{e}^T e + \frac{1}{2} \varepsilon^2 \dot{e}^T M(\phi) e + \frac{1}{2} \varepsilon^2 e^T M(\phi) \dot{e} + \frac{1}{2} \varepsilon^2 e^T \dot{M}(\phi) e + \varepsilon e^T M(\phi) \ddot{e} + \varepsilon e^T \dot{M}(\phi) \dot{e} \\ & + \varepsilon \dot{e}^T M(\phi) \dot{e} + \dot{e}^T M(\phi) \ddot{e} + \frac{1}{2} \dot{e}^T \dot{M}(\phi) \dot{e} \end{aligned} \tag{35}$$

By replacement of Eq. (33) in Eq. (35) and some simplifications, the resulting \dot{H} would be

$$\dot{H} = -\varepsilon e^T K_p e - \dot{e}^T K_D \dot{e} \tag{36}$$

As can be seen, a positive-definite Lyapunov function leads to a negative \dot{H} and guarantees the stability of the given approach. The diagram of the mentioned control algorithm has been illustrated in Fig. 3.

In the next section, the outputs of the Lyapunov-based control have been derived and compared in the lack of uncertainty and disturbance and with considering them.

6.1.1 Lyapunov-based control results in the lack of the disturbances and uncertainties

Firstly, the desired trajectory is designed for the end-effector, which is written in Eq. (36).

$$\begin{cases} X_d = -\frac{1}{10} \sin \frac{t}{3} - \frac{1}{10} \\ Y_d = -\frac{1}{10} \sin \frac{t}{7} \\ Z_d = \frac{1}{10} \cos \frac{t}{2} + \frac{1}{10} \end{cases} \tag{37}$$

As mentioned above, desirable joint angles have been obtained using the JLA path planning method as

$$\phi_d = \phi_{d-1} + (J_E^T L_E J_E + J_A^T L_A J_A + L_S)^{-1} (J_E^T L_E (X - X_1)) \tag{38}$$

$K_D = \text{diag}\{90, 90, 90\}$ and $K_p = \text{diag}\{90, 90, 90\}$ represent proportional and derivative gain matrices, respectively; besides, they are diagonal positive-definite matrices. Joint angles' initial positions are considered as $\phi_0 = [-10 \quad 150 \quad 280]^T$.

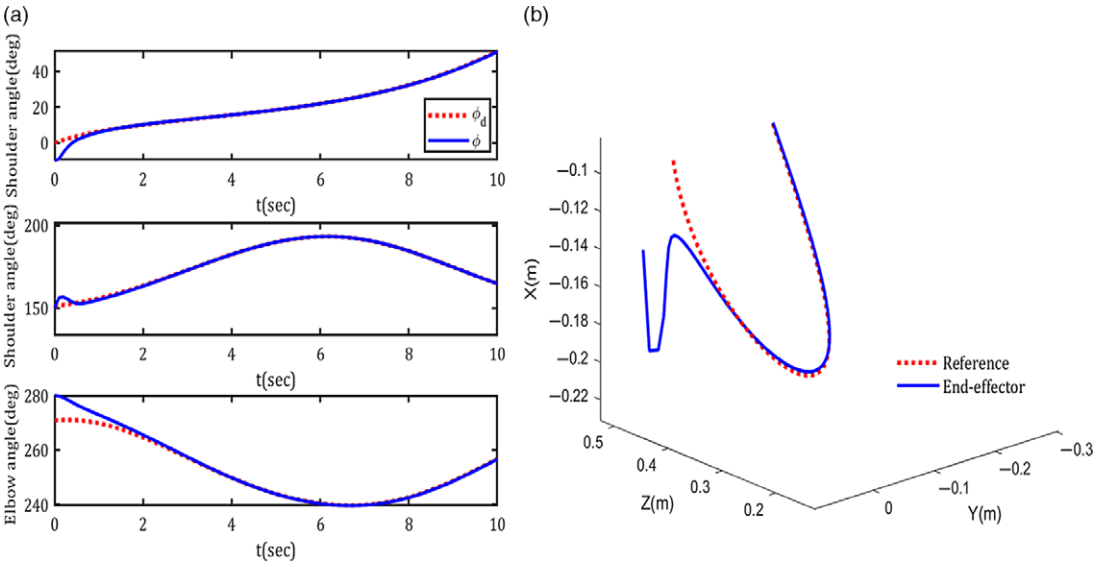


Figure 4. The Lyapunov-based control in the lack of uncertainty and disturbance. (a) Desired and actual joint angles of hand motion. (b) Trajectory tracking of a spatial reference path.

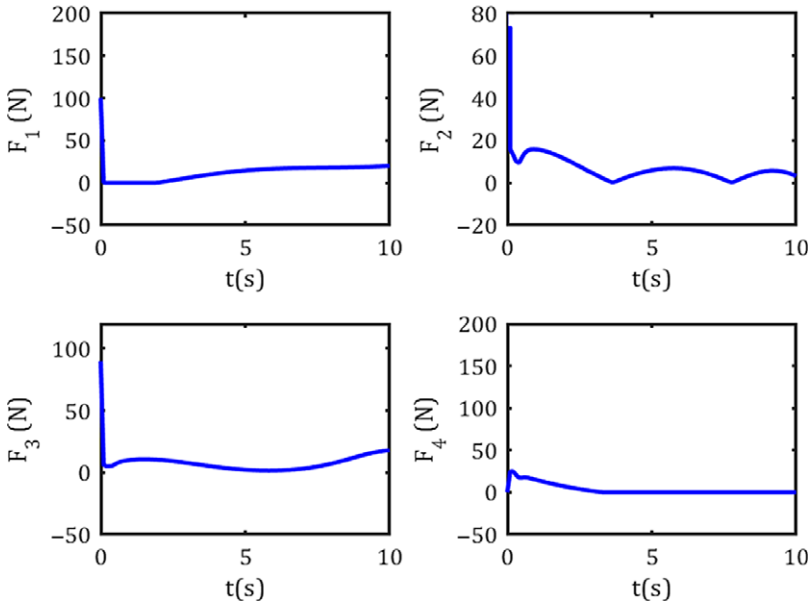


Figure 5. Control inputs of the system in the Lyapunov-based control in the lack of uncertainties and disturbances.

In Fig. 4, joint angles' convergence to the desired angles and path planning of the end-effector in the lack of uncertainties and disturbances are shown.

As can be seen, the whole actual joint angles shift toward the desired joint angles smoothly and in a short time. Similarly, the end-effector tracks the desired 3D path without any deviations. Cable forces as control inputs, which only accept the positive forces for this cable-driven robot, are depicted in Fig. 5.

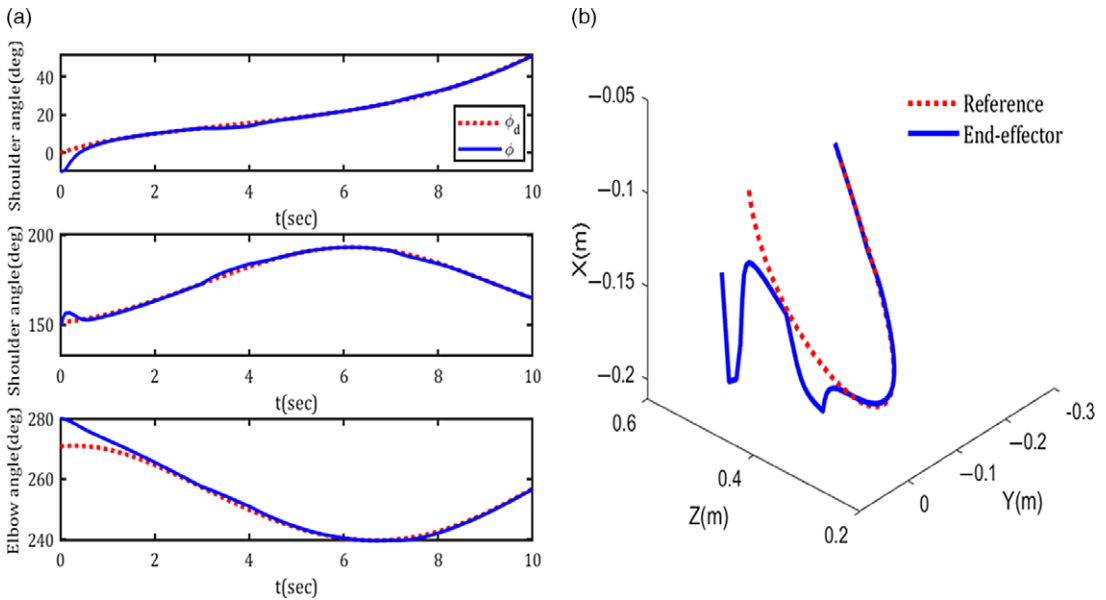


Figure 6. The Lyapunov-based control with considering uncertainty and disturbance. (a) Desired and actual joint angles of hand motion. (b) Trajectory tracking of a spatial reference path.

Obviously, due to the low mass of the links, cables take lower positive values. In Section 6.1.2, the effects of the uncertainties and disturbances are presented on the joints' angles, tracking, and control inputs.

6.1.2. Lyapunov-based control results with considering uncertainty and disturbance

For analysis of the robustness and efficiency of the Lyapunov-based control on this upper limb cable-driven rehabilitating system, the previous plots are derived while taking uncertainty and disturbance into consideration. Uncertainties have been exerted in the mass of the links with 1.1 times more in the interval [23] sec, and disturbances have been used in control inputs with $\Omega = 6 [1 \ 1 \ 1 \ 1]^T \cos \frac{1}{2}$ in [89] sec. K_D and K_P exist as proportional and derivative gain matrices. Also, the initial conditions have been considered as the same in both conditions, with and without uncertainties and disturbances.

Clearly, the Lyapunov-based control does not show robustness with considering uncertainty and disturbance. Besides, considerable tracking errors are occurred and illustrated in Fig. 6. Since uncertainties and disturbances have arrived in the robot, the end-effector goes out of the way, and the position errors increase.

In Fig. 7, cable forces are presented, while it is clear that in the arrival of the uncertainties and disturbances the values have a jump, and more control inputs are needed to control this cable-driven rehabilitating robot.

The results of the Lyapunov-based control with considering uncertainties and disturbances confirm the requirement for a more robust and effective controller due to the tracking errors and higher control efforts; as a result, a new robust controller is introduced in Section 6.2 in comparison with mentioned Lyapunov-based controller.

6.2. Computed-torque-like control with independent-joint compensation

Since a computed-torque control depends on exact dynamic parameters being predefined and cable forces being estimated in real-time to tackle this issue, computed-torque-like control has been introduced. In the presence of uncertainties, a compensator should be considered to minimize their

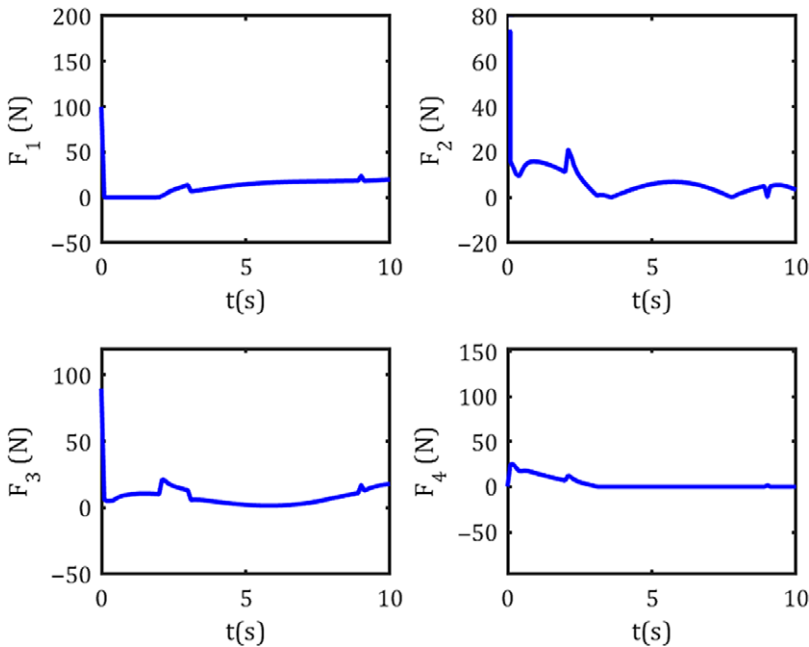


Figure 7. Cable forces in the Lyapunov-based control with considering uncertainty and disturbance.

effects and track errors through its compensation part and robustness to make the end-effector track the reference trajectory precisely. Thus, a computed-torque-like control with independent-joint compensation has been applied to the system, which this new robust controller does not need expensive hardware to take the experimental results in comparison with other robust controllers, and it has indicated its superiorities in tracking in the presence of uncertainties and disturbances.

The general form of the dynamic equation is ref. [26]

$$M(\phi)\ddot{\phi} + B(\phi, \dot{\phi})\dot{\phi} + G(\phi) = T \tag{39}$$

And a computed-torque-like control input is

$$T = \hat{M}(\phi)\mu + \hat{B}(\phi, \dot{\phi})\dot{\phi} + \hat{G}(\phi) \tag{40}$$

$\hat{\cdot}$ indicates nominal parameters. After replacement of Eq. (40) in Eq. (39), and applying some assumptions such as $\hat{M} = I$, $\hat{B} = 0$ and $\hat{G} = 0$, the resulting formulation would be

$$M(\phi)\ddot{\phi} + B(\phi, \dot{\phi})\dot{\phi} + G(\phi) = u \tag{41}$$

To compensate for the consequences of the uncertainties, u is designed as an unknown model uncertainty in the controller.

$$u = -K_D\dot{e} - K_P e + \Delta\mu \tag{42}$$

k_P and k_D present large positive constants. By replacing Eq. (42) in Eq. (41), $\ddot{\phi}$ is derived as

$$\ddot{\phi} = M^{-1}(-K_D\dot{e} - K_P e + \Delta\mu - B\dot{\phi} - G) \tag{43}$$

The error dynamics can be calculated by adding $-\ddot{\phi}_d$ to both sides of Eq. (43).

$$\ddot{e} = M^{-1}(-K_D\dot{e} - K_P e + \Delta\mu - B\dot{\phi} - G) - \ddot{\phi}_d \tag{44}$$

According to some characteristics of robot manipulators and dynamical systems such as

$\|M(\phi)\| \leq \sigma_1, \|G(\phi)\| \leq \sigma_2, \|B(\phi, \dot{\phi})\| \leq \sigma_3 \|\dot{\phi}\|, \phi_d < \alpha_1, \dot{\phi}_d < \alpha_2,$ and $\ddot{\phi}_d < \alpha_3, \|u\|$ yields as

$$\|u\| = \|M\ddot{\phi}_d + B\dot{\phi}_d + G\| \leq \delta_1 + \delta_2 \|\dot{\phi}\| + \delta_3 \|\ddot{\phi}\| = \delta^T \theta \tag{45}$$

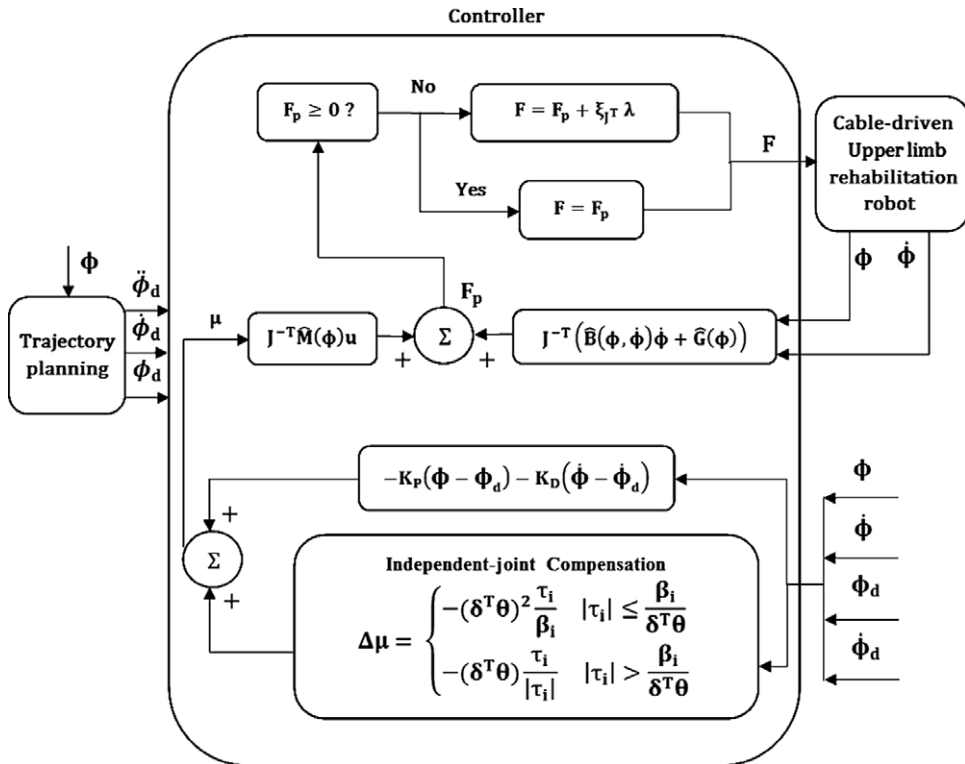


Figure 8. Block diagram of the computed-torque-like control with independent-joint compensation for the upper limb cable-driven rehabilitating system.

where $\delta_1, \delta_2,$ and δ_3 are positive constants, $\delta = [\delta_1 \ \delta_2 \ \delta_3]^T$ and $\theta(\phi, \dot{\phi}) = [1 \ \phi \ \dot{\phi}]^T$. It is noticeable that $\theta(\phi, \dot{\phi})$ is considered as the desired compensation. Then, $\ddot{\phi}_d$ yields from Eq. (45) as

$$\ddot{\phi}_d = M^{-1} (\mu - B\dot{\phi}_d - G) \tag{46}$$

Therefore, the final form of the error dynamics after replacing Eq. (46) would be

$$\ddot{e} = M^{-1} (-K_D \dot{e} - K_P e + \Delta\mu - B\dot{e} - u) \tag{47}$$

Or

$$\begin{bmatrix} \dot{e} \\ \ddot{e} \end{bmatrix} = \begin{bmatrix} 0 & I \\ -M^{-1}k_p & -M^{-1}(k_D + B) \end{bmatrix} \begin{bmatrix} e \\ \dot{e} \end{bmatrix} + \begin{bmatrix} 0 \\ M^{-1} \end{bmatrix} (\Delta\mu - u) \tag{48}$$

The general form of the error dynamics in state space is shown as

$$\dot{e} = Ae + C (\Delta\mu - u) \tag{49}$$

where $A = \begin{bmatrix} 0 & I \\ -M^{-1}k_p & -M^{-1}(k_D + B) \end{bmatrix}$ and $C = \begin{bmatrix} 0 \\ M^{-1} \end{bmatrix}$, and also $e = [e_\phi^T \ \dot{e}_\phi^T]^T$ is the vector of errors and their velocities. To demonstrate the stability of error dynamics, matrix P can be derived through Eq. (50).

$$PA + A^T P = -Q \tag{50}$$

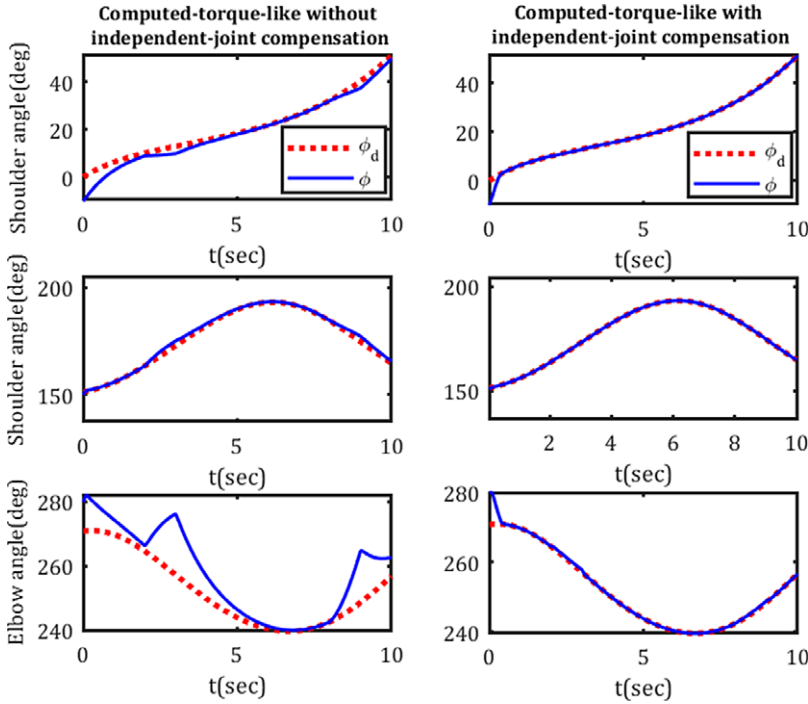


Figure 9. Compared hand joint angles in the computed-torque-like control with independent-joint compensation with considering uncertainty and disturbance.

where $A = \begin{bmatrix} 0 & I \\ -M^{-1}k_p & -M^{-1}(k_D + B) \end{bmatrix}$ and Q represents a positive-definite symmetric matrix. By choice of a P as a positive-definite matrix in Eq. (50), Q can be calculated. A positive-definite Lyapunov function is considered as ref. [26]

$$V = \frac{1}{2}e^T P e + \sum_{i=1}^n \psi_i^{-1} \beta_i \tag{51}$$

And the $\beta_i, i \in \{1, \dots, n\}$ indicates the variable length of the boundary layer

$$\dot{\beta}_i = -\psi_i^{-1} \beta_i, \beta(0) > 0, \psi_i > 0 \tag{52}$$

Making use of Eq. (52) and lower figures of β_i , the tracking error would enter in a smaller residual set. Also, matrix P is defined as

$$P = \begin{bmatrix} \varphi k_p & M \\ M & \varphi M \end{bmatrix} \tag{53}$$

Taking the derivative of V yields [26]

$$\dot{V} = \frac{1}{2} (e^T P \dot{e} + \dot{e}^T P e) - \sum_{i=1}^n \beta_i \tag{54}$$

By replacement of Eq. (49) in \dot{V} it can be concluded that

$$\dot{V} = \frac{1}{2} (Ae + C(\Delta\mu - u))^T P e + e^T P (Ae + C(\Delta\mu - u)) - \sum_{i=1}^n \beta_i \tag{55}$$

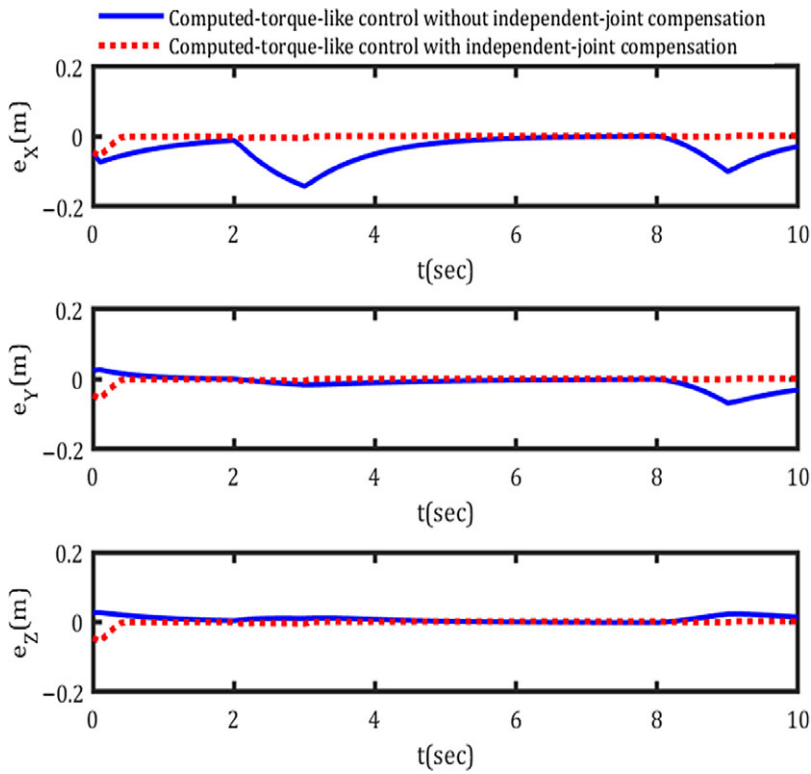


Figure 10. Tracking errors in x , y , and z coordinate in computed-torque-like control with and without the independent-joint compensation with considering uncertainty and disturbance.

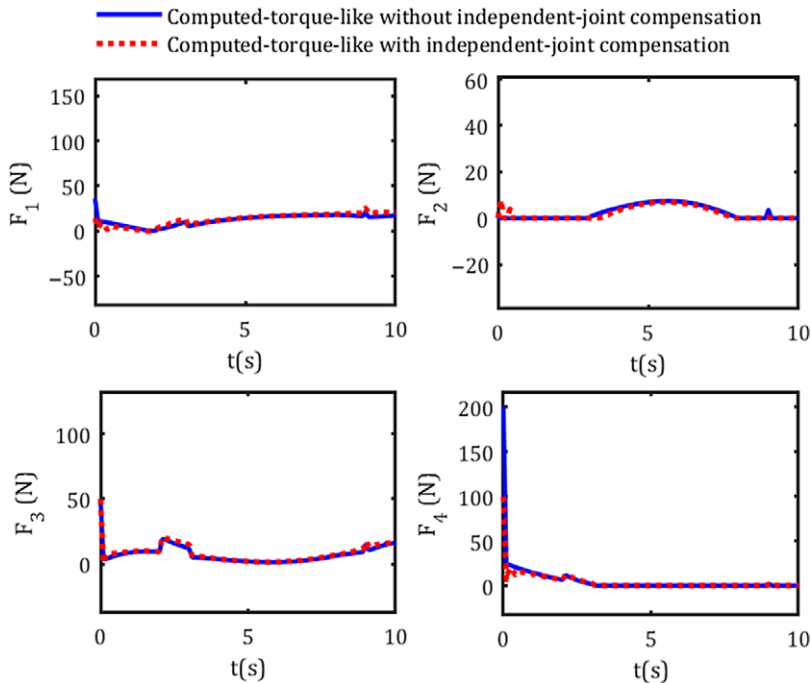


Figure 11. The control inputs in the computed-torque-like control with and without independent-joint compensation with considering uncertainty and disturbance.

Table III. The tracking errors and control inputs in computed-torque-like control in the presence and absence of independent-joint compensation.

	In the absence of the independent-joint compensation	In the presence of the independent-joint compensation
$\int_3^{10} (E_x^2 + E_y^2 + E_z^2) dt$	0.0222	0.0140
$\int_0^{10} F^2 dt$	3.8862×10^3	3.7241×10^3

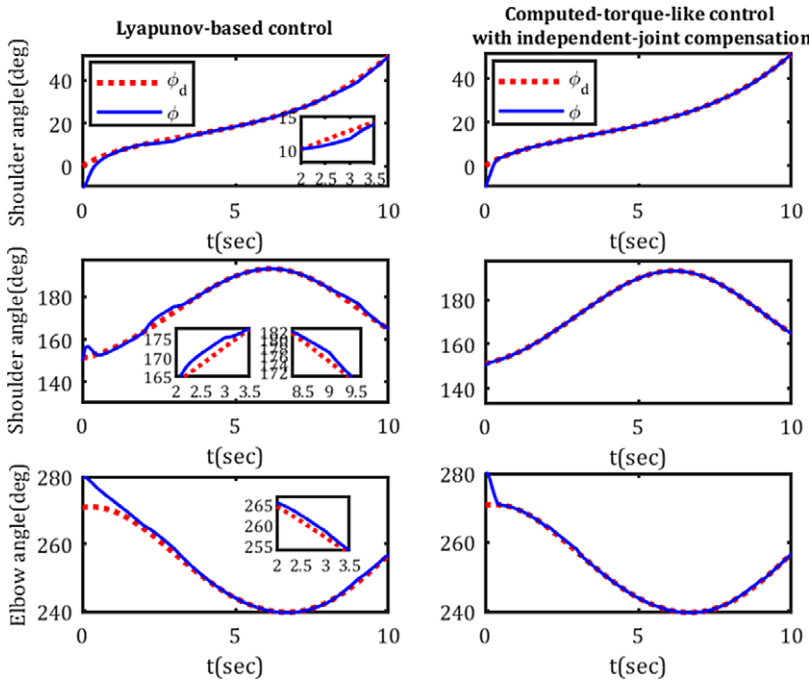


Figure 12. Compared hand joint angles between the Lyapunov-based control and the computed-torque-like control with independent-joint compensation with considering uncertainty and disturbance.

A compensator with independent joint defines the following equation:

$$\Delta\mu = \begin{cases} -(\delta^T\theta)^2 \frac{\tau_i}{\beta_i} & |\tau_i| \leq \frac{\beta_i}{\delta^T\theta} \\ -(\delta^T\theta) \frac{\tau_i}{|\tau_i|} & |\tau_i| > \frac{\beta_i}{\delta^T\theta} \end{cases} \tag{56}$$

where

$$\tau_i = e_i + \varphi_i \dot{e}_i \tag{57}$$

φ_i are positive constant coefficients. Making use of Eq. (50) and some properties such as $\begin{bmatrix} e & \dot{e}^T \end{bmatrix}^T = \begin{bmatrix} \dot{e}^T & e \end{bmatrix}^T$ and $MM^{-1} = I$, \dot{V} turns into

$$\dot{V} = -\frac{1}{2} e^T Q e + e^T P C (\Delta\mu - u) - \sum_{i=1}^n \beta_i \tag{58}$$

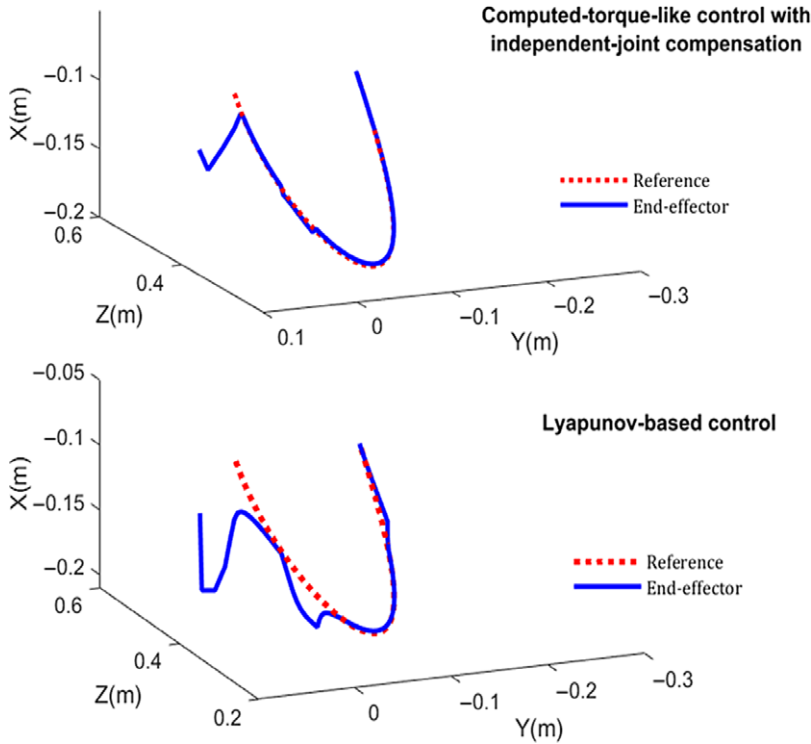


Figure 13. The tracking in the upper limb between the computed-torque-like control with independent-joint compensation and the Lyapunov-based control with considering uncertainty and disturbance.

By taking advantage of Eq. (57), the second term of Eq. (58) would be

$$e^T PC (\Delta\mu - u) = [e^T \quad \dot{e}^T] \begin{bmatrix} \varphi k_p & M \\ M & \varphi M \end{bmatrix} \begin{bmatrix} 0 \\ M^{-1} \end{bmatrix} (\Delta\mu - u) = (e^T + \varphi \dot{e}^T) (\Delta\mu - u) = \tau^T (\Delta\mu - u) \tag{59}$$

Then, \dot{V} yields the following equation:

$$\dot{V} = -\frac{1}{2} e^T Q e + \tau^T (\Delta\mu - u) - \sum_{i=1}^n \beta_i \tag{60}$$

Making use of Cauchy–Schwartz inequalities, \dot{V} is obtained as

$$\dot{V} \leq -\|Q\| \|e\|^2 + \|\tau_i^T\| \|(\Delta\mu - u)\| - \left\| \sum_{i=1}^n \beta_i \right\| \tag{61}$$

μ and $\Delta\mu$ are derived from Eq. (45) and Eq. (56), respectively, and are put into \dot{V} .

$$\dot{V} \leq -\|Q\| \|e\|^2 - \frac{\|\tau_i^T\|^2 \|(\delta^T \theta)\|^2}{\|\beta_i\|} - \|\tau_i^T\| \|(\delta^T \theta)\| - \left\| \sum_{i=1}^n \beta_i \right\| \tag{62}$$

According to the definition of the compensator function in Eq. (56), $\|\tau_i\| = \|\tau_i^T\| \leq \frac{\beta_i}{\delta^T \theta}$ is considered and placed in \dot{V} .

$$\dot{V} \leq -\|Q\| \|e\|^2 - \|\beta_i\| - \left\| \sum_{i=1}^n \beta_i \right\| \tag{63}$$

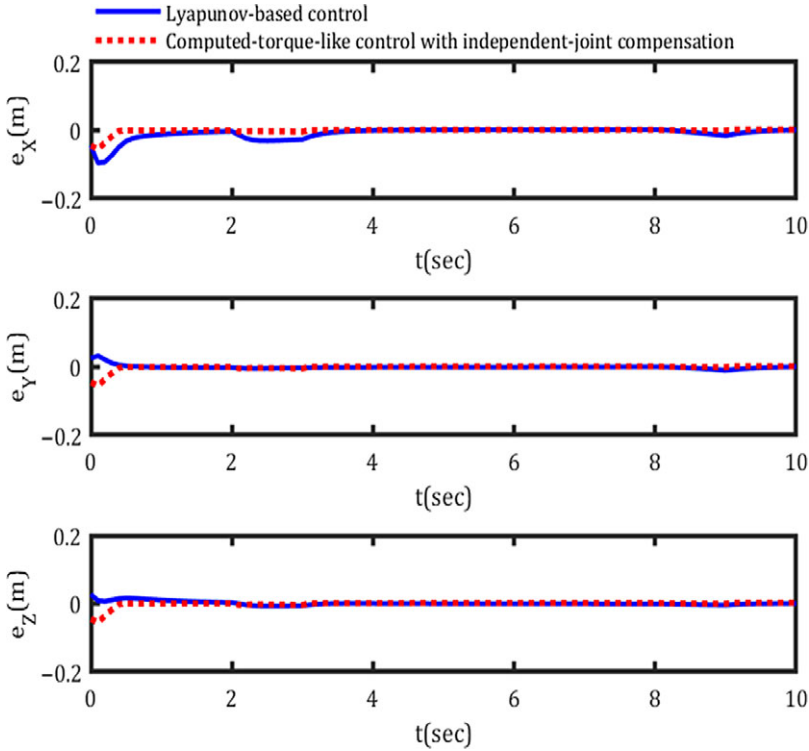


Figure 14. Tracking errors in x , y , and z coordinate in the computed-torque-like control with independent-joint compensation and the Lyapunov-based control with considering uncertainty and disturbance.

Since β_i is an indicator of the variable length of the boundary layer, it is a positive constant. Also, $\sum_{i=1}^n \beta_i$ results in a positive constant; as a result, if $-2 \|\beta_i\| = -2\alpha_1$ and $-\sum_{i=1}^n \beta_i = -\alpha_2$, the final $|\dot{V}|$ would be

$$\dot{V} \leq -\|Q\| \|e\|^2 - 2\alpha_1 - \alpha_2 \leq 0 \tag{64}$$

where α_1 and α_2 show positive constants.

As can be seen, a positive-definite Lyapunov function V leads to a negative definite \dot{V} and ensures the stability of the system. The diagram of the given controller is shown in Fig. 8.

6.2.1 The computed-torque-like control in the presence and absence of the independent-joint compensation

Comparisons between the results of the computed-torque-like control in the presence and absence of the independent-joint compensation are presented, and the efficiency of the proposed compensation is illustrated to guarantee the robustness of this novel method. Similarly, uncertainties are considered in the mass of the links with 1.1 times more in the interval [23] sec, and also, disturbances are exerted to control inputs with $\Omega = 6 [1 \ 1 \ 1 \ 1]^T \cos \frac{1}{2}$ in [89] sec. K_D and K_P define proportional and derivative gain matrices, respectively, as $\text{diag} \{90, 90, 90\}$, and the initial conditions are the same in both conditions, with and without compensator as $\phi_0 = [-10 \ 150 \ 280]^T$.

The joint angles in the computed-torque-like control in the presence and absence of the independent-joint compensation are shown in Fig. 9, and the positive results of applying independent-joint compensation are sensible. The performance of joints' tracking depicts the importance of the compensation existence.

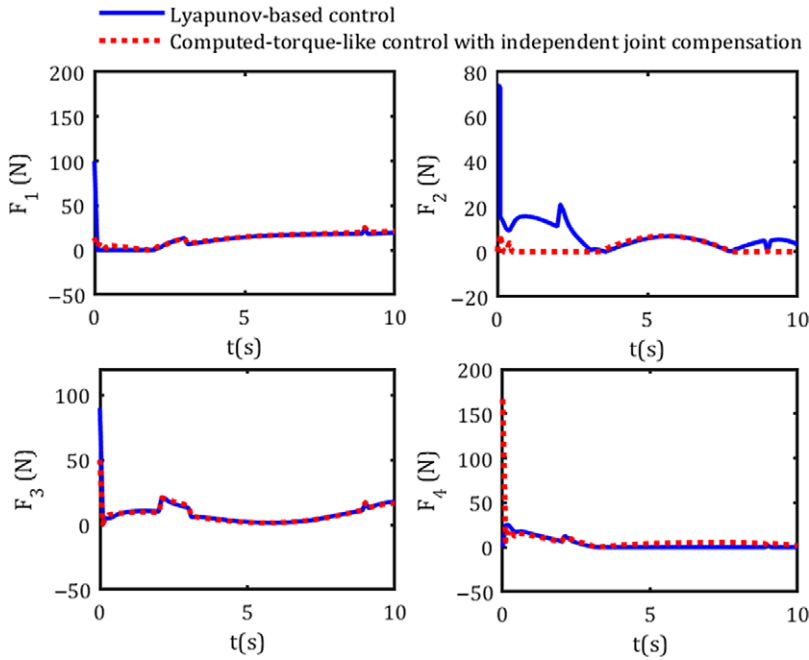


Figure 15. The control inputs in the computed-torque-like control with independent-joint compensation and the Lyapunov-based control with considering uncertainty and disturbance.

Large values of tracking errors in the absence of the independent-joint compensation show the lack of robustness of the system while taking uncertainties and disturbances into consideration.

Furthermore, in Fig. 11, cable forces witnessed larger control efforts in the absence of independent-joint compensation.

Table III represents the tracking errors and control inputs in both conditions.

According to the numerical figures, consideration of the independent-joint compensation improves the tracking error and the total control inputs with about 36.94% and 4.18%, respectively, and this novel controller properly acts as a robust controller. We keep this robust control in the next section to compare it with the Lyapunov-based control.

6.3. A comparison of the computed-torque-like control with independent-joint compensation and the lyapunov-based control with considering the uncertainty and disturbance

For demonstrating the robustness of the proposed control method with considering the uncertainties and disturbances, uncertainties have arrived in the mass of the links with 1.1 times more in the interval [23] sec, and disturbances are considered in control inputs with $\Omega = 6 [1 \ 1 \ 1 \ 1]^T \cos \frac{1}{2}$ in [89] sec. Besides, K_D and K_P are indicators of proportional and derivative gain matrices as $\text{diag} \{90, 90, 90\}$ and $\text{diag} \{90, 90, 90\}$, respectively, and the same initial conditions in both controllers are as $\phi_0 = [-10 \ 150 \ 280]^T$. The results are all derived and compared thoroughly in the same conditions.

Initially, as can be seen in Fig. 12, actual joint angles in computed-torque-like control with independent-joint compensation converged to the desired ones in a short time and a smooth way. Besides, none of the actual generalized coordinates have deviated from the desired signals, while in the Lyapunov-based control all of the actual joint angles do not show a proper function and move away at the moments of uncertainties and disturbances existence.

Table IV. The tracking errors and the control inputs in the Lyapunov-based control and the computed-torque-like control with independent-joint compensator.

	Computed-torque-like control with independent-joint compensation	Lyapunov-based control
$\int_3^{10} (E_x^2 + E_y^2 + E_z^2) dt$	0.0140	0.0195
$\int_0^{10} F^2 dt$	3.4184×10^3	1.1103×10^4

A desirable trajectory tracking of the computed-torque-like control with independent-joint compensation is representative of the robustness of this control algorithm with considering uncertainties and disturbances and depicts a better performance, which is shown in Fig. 13.

According to Fig. 14, in the proposed controller the tracking errors converge to zero in a short time and guarantee the stability of the robot, while in the Lyapunov-based control, errors in x coordinate illustrate the deviation in the moments of uncertainties and disturbances.

In Fig. 15, cables experience higher forces in the Lyapunov-based control against uncertainties and disturbances, especially in cable 2; furthermore, motors need larger energy used to maintain the tracking, and also, higher cable tensions are needed.

Numerical figures regarding the overall tracking errors and the control inputs for both control algorithms are calculated in Table IV.

The numerical figures in Table IV demonstrate a 28.21% and 69.22% improvement in overall tracking errors and the control inputs in the computed-torque-like control with independent-joint compensation. As a result, the proposed robust control algorithm has an acceptable performance in tracking and needs less control input against uncertainties and disturbances.

7. Conclusion

This research represented a three-DOF upper limb cable-driven rehabilitating robot containing four motors in spatial path planning. Dynamic equations were exploited through the Lagrangian method. Afterward, positive cable tensions were obtained through null space. Since one of the vital constraints in this CDRR was holding joint angles in a definite lower and upper limit, the path planning was derived through the new joint limit-avoidance approach, and the results' improvements were revealed.

A novel robust control scheme of the proposed upper limb CDRR in a 3D path and its functionality with considering uncertainties and disturbances were the chief goals of this research. Consequently, the comparative outputs between the Lyapunov-based control and the computed-torque-like control with independent-joint compensation in the presence of uncertainties and disturbances were compared. The efficiency of the proposed robust control method was demonstrated by a 28.21% improvement in tracking. Furthermore, cable tensions as control inputs experienced an improvement with about 69.22%, and motors required less power to move and control the robot.

Finally, one of the potential research plans about this cable-driven rehabilitation system can be the consideration of the elasticity of the cables in dynamic modeling. Different optimization algorithms can be also applied to the robot to extract the least and more efficient positive control inputs. Moreover, to validate the theoretical results, the system can be tested in real time and a comparison can be drawn between the results.

References

- [1] J. Niu, Q. Yang, X. Wang and R. Song, "Sliding mode tracking control of a wire-driven upper-limb rehabilitation robot with nonlinear disturbance observer," *Front. Neurol.* **8**, 646 (2017).
- [2] J. Wang, W. Li, W. Chen and J. Zhang, "Motion Control of a 4-DOF Cable-Driven Upper Limb Exoskeleton," *In: 14th IEEE Conference on Industrial Electronics and Applications (ICIEA)* (IEEE, 2019) pp. 2129–2134.

- [3] S. K. Mustafa and S. K. Agrawal, "On the force-closure analysis of n-DOF cable-driven open chains based on reciprocal screw theory," *IEEE Trans. Robot.* **28**(1), 22–31 (2011).
- [4] X. Cui, W. Chen, G. Yang and Y. Jin, "Closed-Loop Control for a Cable-driven Parallel Manipulator with Joint Angle Feedback," **In: IEEE/ASME International Conference on Advanced Intelligent Mechatronics (IEEE, 2013)** pp. 625–630.
- [5] W. Chen, X. Cui, G. Yang, J. Chen and Y. Jin, "Self-feedback motion control for cable-driven parallel manipulators," *Proc. Inst. Mech. Eng. C* **228**(1), 77–89 (2014).
- [6] C. L. Jones, F. Wang, R. Morrison, N. Sarkar and D. G. Kamper, "Design and development of the cable actuated finger exoskeleton for hand rehabilitation following stroke," *IEEE/ASME Trans. Mechatron.* **19**(1), 131–140 (2012).
- [7] D. Zanotto, G. Rosati, S. Minto and A. Rossi, "Sophia-3: A semiadaptive cable-driven rehabilitation device with a tilting working plane," *IEEE Trans. Robot.* **30**(4), 974–979 (2014).
- [8] I. Gaponov, D. Popov, S. J. Lee and J.-H. Ryu, "Auxilio: A portable cable-driven exosuit for upper extremity assistance," *Int. J. Control Autom. Syst.* **15**(1), 73–84 (2017).
- [9] J. Niu, Q. Yang, G. Chen and R. Song, "Nonlinear Disturbance Observer Based Sliding Mode Control of a Cable-driven Rehabilitation Robot," **In: International Conference on Rehabilitation Robotics (ICORR)** (IEEE, 2017) pp. 664–669.
- [10] K. P. Tee, R. Yan and H. Li, "Adaptive Admittance Control of a Robot Manipulator Under Task Space Constraint," **In: IEEE International Conference on Robotics and Automation** (IEEE, 2010) pp. 5181–5186.
- [11] Y. Mao and S. K. Agrawal, "A Cable Driven Upper Arm Exoskeleton for Upper Extremity Rehabilitation," **In: IEEE International Conference on Robotics and Automation** (IEEE, 2011) pp. 4163–4168.
- [12] H. Mehdi and O. Boubaker, "Stiffness and impedance control using Lyapunov theory for robot-aided rehabilitation," *Int. J. Soc. Robot.* **4**(1), 107–119 (2012).
- [13] M. Yamashita, "Robotic rehabilitation system for human upper limbs using guide control and manipulability ellipsoid prediction," *Proc. Technol.* **15**, 559–565 (2014).
- [14] A. M. Khan, D.-w. Yun, M. A. Ali, J. Han, K. Shin and C. Han, "Adaptive Impedance Control for Upper Limb Assist Exoskeleton," **In: IEEE International Conference on Robotics and Automation (ICRA)** (IEEE, 2015) pp. 4359–4366.
- [15] W. Chen, X. Cui, J. Zhang and J. Wang, "A cable-driven wrist robotic rehabilitator using a novel torque-field controller for human motion training," *Rev. Sci. Instrum.* **86**(6), 065109 (2015).
- [16] Q. Yang, J. Niu and R. Song, "Admittance Control of a 3-DOF Cable-driven Rehabilitation Robot for Upper-Limb in Three Dimensional Workspace," **In: 2nd International Conference on Advanced Robotics and Mechatronics (ICARM)** (IEEE, 2017) pp. 445–449.
- [17] E. L. Oyman and M. S. Arslan, "Impedance-Based Control of a Cable Driven Rehabilitation Robot," **In: 6th International Conference on Control Engineering & Information Technology (CEIT)** (IEEE, 2018) pp. 1–6.
- [18] W. Ni, H. Li, Z. Jiang, B. Zhang and Q. Huang, "Motion and force control method of 7-DOF cable-driven rehabilitation exoskeleton robot," *Assembly Autom.* **38**(5), 595–605 (2018).
- [19] H. Xiong and X. Diao, "Motion Control of Cable-Driven Rehabilitation Devices with Large Deformation Cables," **In: IEEE International Conference on Cyborg and Bionic Systems (CBS)** (IEEE, 2018) pp. 537–543.
- [20] Q. Fang, G. Li, T. Xu, J. Zhao, H. Cai and Y. Zhu, "A simplified inverse dynamics modelling method for a novel rehabilitation exoskeleton with parallel joints and its application to trajectory tracking," *Math. Probl. Eng.* **2019**(5), 1–10 (2019).
- [21] C.-T. Chen, W.-Y. Lien, C.-T. Chen, M.-J. Twu and Y.-C. Wu, "Dynamic modeling and motion control of a cable-driven robotic exoskeleton with pneumatic artificial muscle actuators," *IEEE Access* **8**, 149796–149807 (2020).
- [22] Q. Yang, C. Xie, R. Tang, H. Liu and R. Song, "Hybrid active control with human intention detection of an upper-limb cable-driven rehabilitation robot," *IEEE Access* **8**, 195206–195215 (2020).
- [23] A. Izadbakhsh and S. Khorashadizadeh, "Polynomial-based robust adaptive impedance control of electrically driven robots," *Robotica* **39**(7), 1181–1201 (2021).
- [24] M. M. Fateh and S. Khorashadizadeh, "Optimal robust voltage control of electrically driven robot manipulators," *Nonlinear Dynam.* **70**(2), 1445–1458 (2012).
- [25] N. S. Seyfi and A. K. Khalaji, "Robust control of a cable-driven rehabilitation robot for lower and upper limbs," *ISA Trans.* **8**(5), 256 (2021).
- [26] B. Siciliano and O. Khatib. *Springer Handbook of Robotics* (Springer, 2016).

Appendix

Mass matrix $M(\phi)$, centrifugal and Coriolis forces vector $B(\phi, \dot{\phi})$, and gravitational forces $G(\phi)$ in the dynamic formulation in Eq. (A5) are defined below. Mass matrix is presented as

$$M = \begin{bmatrix} M_{11} & M_{12} & M_{13} \\ M_{21} & M_{22} & M_{23} \\ M_{31} & M_{32} & M_{33} \end{bmatrix} \quad (\text{A1})$$

The arrays of the mass matrix are defined below.

$$M_{11} = \frac{I_{2z}}{2} + \frac{I_{3z}}{2} + \frac{I_{3z} \cos(2\phi_2 + 2\phi_3)}{2} + \frac{l_a^2 m_f}{8} + \frac{l_a^2 m_h}{2} + \frac{l_f^2 m_h}{8} + \frac{I_{2z} \cos(2\phi_2)}{2} + \frac{l_a^2 m_f \cos(2\phi_2)}{8} + \frac{l_a^2 m_h \cos(2\phi_2)}{2} + \frac{l_a^2 m_h \cos(2\phi_2 + 2\phi_3)}{8} + \frac{l_a l_f m_h \cos(\phi_3)}{2} + \frac{l_a l_f m_h \cos(2\phi_2 + \phi_3)}{2} \tag{A2}$$

$$M_{12} = 0 \tag{A3}$$

$$M_{13} = 0 \tag{A4}$$

$$M_{21} = 0 \tag{A5}$$

$$M_{22} = I_{2z} + I_{3z} + \frac{l_a^2 m_f}{4} + l_a^2 m_h + \frac{l_f^2 m_h}{4} + l_a l_f m_h \cos(\phi_3) \tag{A6}$$

$$M_{23} = \frac{l_f^2 m_h}{4} + \frac{l_a l_f m_h \cos(\phi_3)}{2} I_{3z} \tag{A7}$$

$$M_{31} = 0 \tag{A8}$$

$$M_{32} = \frac{l_f^2 m_h}{4} + \frac{l_a l_f m_h \cos(\phi_3)}{2} + I_{3z} \tag{A9}$$

$$M_{33} = \frac{l_f^2 m_h}{4} + I_{3z} \tag{A10}$$

Here centrifugal and Coriolis forces vector is shown in Eq. (A11).

$$B = \begin{bmatrix} B_1 \\ B_2 \\ B_3 \end{bmatrix} \tag{A11}$$

Each array of matrix $B(\phi, \dot{\phi})$ is explained as

$$B_1 = -\dot{\phi}_1 \dot{\phi}_2 \left(I_{3z} \sin(2\phi_2 + 2\phi_3) + I_{2z} \sin(2\phi_2) + \frac{l_f^2 m_h \sin(2\phi_2 + 2\phi_3)}{4} + \frac{l_a^2 m_f \sin(2\phi_2)}{4} + l_a^2 m_h \sin(2\phi_2) + l_a l_f m_h \sin(2\phi_2 + \phi_3) \right) - \dot{\phi}_1 \dot{\phi}_2 \left(I_{3z} \sin(2\phi_2 + 2\phi_3) + \frac{l_f^2 m_h \sin(2\phi_2 + 2\phi_3)}{4} + \frac{l_a l_f m_h \sin(\phi_3)}{2} + \frac{l_a l_f m_h \sin(2\phi_2 + \phi_3)}{2} \right) \tag{A12}$$

$$B_2 = \frac{I_{2z} \dot{\phi}_1^2 \sin(2\phi_2)}{2} + \frac{I_{3z} \dot{\phi}_1^2 \sin(2\phi_2 + 2\phi_3)}{2} + \frac{\dot{\phi}_1^2 l_a^2 m_f \sin(2\phi_2)}{8} + \frac{\dot{\phi}_1^2 l_a^2 m_h \sin(2\phi_2)}{2} + \frac{\dot{\phi}_1^2 l_f^2 m_h \sin(2\phi_2 + 2\phi_3)}{8} - \frac{l_a l_f m_h \dot{\phi}_3^2 \sin(\phi_3)}{2} + \frac{l_a l_f m_h \dot{\phi}_1^2 \sin(2\phi_2 + \phi_3)}{2} - l_a l_f m_h \dot{\phi}_2 \dot{\phi}_3 \sin(\phi_3) \tag{A13}$$

$$B_3 = \left(\frac{I_{3z} \sin(2\phi_2 + 2\phi_3)}{2} + \frac{l_f^2 m_h \sin(2\phi_2 + 2\phi_3)}{8} + \frac{l_a l_f m_h \sin(\phi_3)}{4} + \frac{l_a l_f m_h \dot{\phi}_1^2 \sin(2\phi_2 + \phi_3)}{4} + \frac{\dot{\phi}_2^2 l_a l_f m_h \sin(\phi_3)}{2} \right) \tag{A14}$$

The gravitational forces vector $G(\phi)$ and its arrays are shown as

$$G = \begin{bmatrix} G_1 \\ G_2 \\ G_3 \end{bmatrix} \tag{A15}$$

$$G_1 = \frac{-g \sin(\phi_1) (l_a m_f \cos(\phi_2) + 2l_a m_h \cos(\phi_2) + l_f m_h \cos(\phi_2 + \phi_3))}{2} \tag{A16}$$

$$G_2 = \frac{-g \cos(\phi_1) (l_a m_f \sin(\phi_2) + 2l_a m_h \sin(\phi_2) + l_f m_h \sin(\phi_2 + \phi_3))}{2} \tag{A17}$$

$$G_3 = \frac{-g l_f m_h \sin(\phi_2 + \phi_3) \cos(\phi_1)}{2} \tag{A18}$$